High-Quality Whispering-Gallery-Mode Lasing from Cesium Lead Halide Perovskite Nanoplatelets

Zhang, Qing; Su, Rui; Liu, Xinfeng; Xing, Jun; Sum, Tze Chien; Xiong, Qihua

2016

Zhang, Q., Su, R., Liu, X., Xing, J., Sum, T. C., & Xiong, Q. (2016). High-Quality Whispering-Gallery-Mode Lasing from Cesium Lead Halide Perovskite Nanoplatelets. Advanced Functional Materials, 26(34), 6238-6245.

https://hdl.handle.net/10356/84080

https://doi.org/10.1002/adfm.201601690

Submitted to ADVANCED MATERIALS

DOI: (Please add manuscript number)
Article type: Communication

High Quality Whispering-Gallery-Mode Lasing from Cesium Lead Halide Perovskite Nanoplatelets

By Qing Zhang, Rui Su, Xinfeng Liu, Jun Xing, Tze Chien Sum, Qihua Xiong **

[*] Dr. Q. Zhang, R. Su, Dr. J. Xing
Division of Physics and Applied Physics, School of Physical and Mathematical Sciences, Nanyang Technological University, Singapore 637371

Dr. X. F. Liu
Division of Physics and Applied Physics, School of Physical and Mathematical Sciences, Nanyang Technological University, Singapore 637371;
National Center for Nanoscience and Technology, Chinese Academy of Sciences, Beijing 100190, China.

Prof. T. C. Sum
Division of Physics and Applied Physics, School of Physical and Mathematical Sciences, Nanyang Technological University, Singapore 637371;
Energy Research Institute @ NTU (ERI@N), Nanyang Technological University, 50 Nanyang Drive, Singapore 637553;
Singapore-Berkeley Research Initiative for Sustainable Energy, 1 Create Way, Singapore 138602, Singapore.
Email: tzechien@ntu.edu.sg

Prof. Q. H. Xiong
Division of Physics and Applied Physics, School of Physical and Mathematical Sciences, Nanyang Technological University, Singapore 637371;
NOVITAS, Nanoelectronics Centre of Excellence, School of Electrical and Electronic Engineering, Nanyang Technological University, Singapore, 639798
Email: Qihua@ntu.edu.sg

Keywords: Cesium Lead Halide; Perovskite; Nanolaser; Whispering-Gallery-Mode; Van der Waals Epitaxy; Microcavity;

The fundamental and technological progress in materials sciences and condensed matter physics has led to the revolution and evolution of a variety of functional devices that modernize our society and social life. Further advances, however, will largely depend on novel materials, especially emergent materials with multifunctionality and their advanced applications. Recently, lead halide perovskite has regained attentions for its big success in photovoltaic.[1-3] As a direct band-gap semiconductor, lead halide perovskite family exhibits outstanding optical and emission properties, which are promising for flexible, low-cost photonic devices including laser, light-emission devices and photodetector, *etc*.[4-8] Through structural engineering and composition tuning, the emission colour of lead halide perovskite can be tuned from UV to NIR as well as a large scale of exciton binding energy tailorable from several to several hundreds of meV.[2, 9, 10] Together with well-controlled exciton behaviour, the cubic lattice of the type of materials promises the achievement of high-quality factor single crystalline Fabry-Pérot and whispering-gallery-mode cavities.[4, 11] In this regard, lead halide perovskite not only provides a perfect platform for us to study exciton-photon interaction from weak to strong region in fundamental level, but also opens a new territory of functional and high-efficient optoelectronic devices to complement traditional inorganic semiconductors[4, 5, 12, 13].

Single crystalline semiconductor optical micro/nano-cavities with high quality factor (Q) and small modal volume are important for development of microscopic coherent laser source for on-chip optical communications, high-density storage and super-resolution imaging in life sciences.[14] Semiconductor nanostructures, such as single crystalline nanowires and microdisks, can serve as both gain media and optical microcavities confined by their facets, which is particularly promising for high-quality small size laser sources.[15-18] However, constrained by exciton binding energy and thermal fluctuation, only handful wide-band traditional semiconductors such as ZnO and GaN have stable and active excitons at room

temperature (Supporting Information, Fig. S1). In visible luminescent II-VI/III-V semiconductors such as CdSe, ZnTe, *etc*, exciton dislocates at room temperature because of thermal fluctuation and thus free carrier emission dominates which has larger optical loss than exciton emission. In several ionic systems such as Cu_2O[19], CuCl and CuBr, E_b is as large as 80-100 meV, while emission energy is still beyond 3.2-4.0 eV. The spectra coherence, one of the most important characteristic of a laser device, is evaluated by lasing linewidth. According to Schawllow-Townes equation, the lasing linewidth is constrained by cavity *Q* and gain value of semiconductor, and the coupling efficiency of spontaneous emission into lasing process.[20] Till now, the lasing linewidth $\delta\lambda_1$ of visible nano/microlaser based on single crystalline II-VI semiconductor compounds nanostructures is lower than ~0.25 nm (Supporting Information, Tab. S1; Supporting Information Note 1)[11, 21-24]. Although two-dimensional transition metal dichalcogenide has recently been shown with exciton binding energy on the order of ~ 1 eV at visible region, the thickness of mono- or few-layer structures (sub-5 nm) is far below diffraction limit and unable to support a low-loss active cavity by themselves[25]. The lasing of two dimensional materials was achieved at low temperature (~ 130 K) and other optical cavities were necessary, which limits the technologically applications of the lasers[25]. In organic semiconductors, Frenkel excitons are dominated with binding energy of several hundreds meV, while the materials stability and poor crystallinity are big concerns.[26, 27]

Recently, a room temperature lasing from single crystalline organic-inorganic $CH_3NH_3PbBr_3$ perovskite nanowires was proved. The lasing linewidth $\delta\lambda_l$ ~ 0.21 nm and 0.23 nm at 520 and 790 nm respectively, [4, 11] which is slightly higher than that of II-VI/III-V luminescent semiconductor compounds. Compared with the organic-inorganic lead halide perovskites[5, 7, 8], all-inorganic lead halide, such as $CsPbX_3$, (X=I, Br, Cl), exhibit better stability, relatively larger exciton binding energy and higher emission efficiency (~ 90%)[28, 29],

which promises for coherent and quantum light source[29]. Nonetheless, solution-processing synthesized colloidal $CsPbX_3$ quantum dots (CQDs) film random laser still suffers from low spectra linewidth $\delta\lambda_l$ ~ 5 nm, caused by significant scattering loss[30]. The lasing spectra coherence is improved ($\delta\lambda_l$ ~ 2 nm) through embedding the CQDs into whispering-gallery-mode silica spheres cavities; however the spontaneous emission coupled into the lasing processes is not sufficient and the spontaneous emission background is still a problem for real applications[22]. A single crystalline cesium lead halide microcavities functioned as both gain materials and optical feedback suppliers can address both problems simultaneously. However, till now most of $CsPbX_3$ perovskite nanostrctures (nanocrystals, nanowires and nanosheets, *etc*) were prepared by solution processing methods and the sample thickness is smaller than 20 nm.[31-33] According to optical diffraction law, the $CsPbX_3$ nanostructures cannot form effective optical cavities and provide effective optical feedback to support amplification and lasing actions by themselves.

In this work, we synthesized high-quality single crystalline all-inorganic cesium lead halide $CsPbX_3$ (X=Cl, Br, I) nanoplatelets with micro-scale edge length and sub-wavelength thickness using vapour-phase van der Waals epitaxy method. The as-grown luminescent perovskite show intense, narrow-band, tunable absorption and emission properties in the whole visible spectra region. Temperature-dependent absorption spectroscopy studies demonstrate that the exciton binding energy for $CsPbCl_3$, $CsPbBr_3$ is 72 meV and 38 meV respectively. Multi-colour (400-700 nm), low-threshold (~ 2.2 μJ/cm^2), high quality lasing action is realized in the naturally formed single crystalline WGM microcavities. The lasing mode linewidth is ~ 0.14-0.15 nm, which is so far the highest among single crystalline semiconductor microcavities in visible region.

Cesium lead halide $CsPbX_3$ perovskite nanoplatelets were grown on muscovite mica substrates using vapor transport chemical vapor deposition (CVD) method as previous

literature works introduced.[34-36] Fig. 1a illustrates typical optical images of $CsPbBr_3$ nanoplatelets grown on mica substrate. The nanoplatelets are featured with well-defined square shapes which are determined by the crystalline structure of $CsPbBr_3$. The predominant square shapes of nanoplatelets originate from intrinsic cubic phase under high temperature (*i.e.,* > 400 K)[37]. The square nanoplatelets are well oriented at multiples of 90^0, which suggest the epitaxial nature of $CsPbBr_3$ crystals on mica. The growth mechanism is believed to be van der Waals epitaxy, which has been previously discussed in detail in planar and nonplanar structures grown on van der Waals substrates such as mica, graphene or boron nitride by vapor phase or solution methods[10, 34-36, 38-42]. The lateral dimension of the perovskites nanoplatelets are ranging from 1.0 to 20.0 μm. Due to diffraction between the top and bottom facets, the perovskite nanoplatelets show rich colors dependent on the thickness ranging from 50.0 to 300.0 nm, which can be correlated from the optical images and atomic force microscopy (AFM) (Fig. 1b). The size distribution may be due to the surface non-uniformity of mica substrate. The perovskite nanoplatelets also show a highly smooth surface with a surface roughness of only ~2.0 nm as indicated by AFM measurement (Fig. 1b), which is perfectly flat in optical level. Similar well-defined structures can also be obtained on $CsPbX_3$ with halide composition modulation, such as by altering Cl/Br ratio to obtain $CsPb(Cl/Br)_3$ nanoplatelets and Br/I ratio to obtain $CsPb(Br/I)_3$ nanoplatelets. The detailed growth condition is summarized in Supplementary Table 2. These $CsPbX_3$ nanoplatelets were further characterized by powder X-ray diffraction (XRD) (Fig. 1c) in θ–θ geometry, which means that only planes parallel to substrate surface contribute to XRD patterns. Three peaks, which correspond to (100), (110) and (200) planes, can be well indexed to the cubic phase of $CsPbX_3$ perovskites, while the other peaks originate from the mica substrate and the source materials. Furthermore, these three peaks show blue shifts from $CsPbCl_3$ to $CsPbI_3$, which is due to the increasing lattice constant. Three types of crystalline structures are reported in

$CsPbX_3$, including orthorhombic, tetragonal (*ie*., 88°C for $CsPbBr_3$), and cubic polymorphs (*ie*.,130°C for $CsPbBr_3$).[43, 44] While only cubic phase expected to exist above 400 K, is observed for all the samples even at room temperature. In $CsPbX_3$ quantum dots, similar phenomenon was found which was attributed to high growth temperature and large surface energy.[29]

All the cesium lead halide perovskites are direct band gap semiconductors. In $CsPbX_3$ perovskites, band edge states are mainly determined by inorganic PbX_6^+ octahedron. The conduction and valence band forms due to hybridization states between cation Pb and anion X orbital[45]. When the halide elemental weight increases from Cl to I, the bond strength between Pb and X decreases and then the valence and conduction band moves closer, which leads to the decreasing of optical band gap from 412 nm ($CsPbCl_3$) to 700 nm ($CsPbI_3$) (Fig. 1d).[45, 46] The as-synthesized $CsPbCl_3$, $CsPbBr_3$ nanoplatelets show a strong and narrow excitonic absorption peak with full width at half maximum (FWHM) of 80.0 meV (7.0 nm) and 65.0 meV (15.0 nm) at room temperature, respectively, which implies a large exciton binding energy. The room temperature PL spectra and image reveal that $CsPbCl_3$, $CsPbBr_3$, and $CsPbI_3$ emit light at 3.00 eV (412 nm, FWHM ~ 8.0 nm, blue), 2.35eV (527 nm, FWHM~ 20.0 nm, green), and 1.77eV (700 nm, FWHM ~30.0 nm, red), respectively. For given material, apart from intrinsic exciton transition and exciton-phonon scattering the exciton linewidth can be broaden by disorder, surface, defects, *etc*. [47, 48] The PL FWHM (8.0-30.0 nm) of $CsPbX_3$ nanoplatelets is smaller than that of highly luminescent $CsPbX_3$ CQDs (12.0-42.0 nm) at room temperature, which suggests the high quality and good optical/excitonic properties of as-grown nanoplatelets[29, 49, 50]. Bandgap engineering is achieved by compositional modulation, specifically, by tuning the Cl/Br ratio for the 410-527 nm range, and Br/I ratio for 527-700 nm range, which almost covers the entire visible spectral region (Supporting Information, Fig. S2).

A detailed temperature-dependent absorption spectroscopy was conducted to study the exciton dynamics of the inorganic semiconductor perovskites. Fig. 1e shows the band edge absorption spectroscopy of $CsPbCl_3$ as the temperature decreases from 350 to 77 K as a typical example. Temperature dependent absorption spectroscopy of $CsPbBr_3$ could be obtained in Supporting Information (Fig. S3). Strong exciton peak near the band edge can be resolved even at 350 K. In general, spectra linewidth of exciton absorption can be attributed to inhomogeneous and homogenous broadening.[47, 48] The inhomogeneous broadening mostly due to disorder is temperature-independent, which will not be considered here. On the other hand, the homogenous broadening includes two contributions: 1) nature population relaxation of excited states including both of radiative and non-radiative recombination; 2) elastic scattering events such as exciton-exciton, exciton-phonon processing. As shown in Fig. 1f, when the temperature decreases from 310 to 77 K, the exciton absorption peak becomes narrower; the peak intensity increases (supplementary information Fig. S3). The phenomena suggest that exciton dislocation is predominated by exciton-phonon inelastic scattering.[48] Based on the model, the linewidth of exciton absorption peak can be written as a function of temperature *via* $\delta V = \delta V_0 + V_T e^{-E_B / k_B T}$. In the equation, $\delta V, \delta V_0, V_T, E_B, k_B$ is the bandwidth of exciton peak, temperature-independent broadening, temperature dependent broadening, exciton binding energy and Boltzmann constant, respectively.[48] As shown in Fig. 2a, the FWHM of exciton peaks for $CsPbCl_3$ and $CsPbBr_3$ are extracted out, which can be well fitted by the above equations (Fig. 1f, Supporting information Fig. S3). Exciton binding energy E_b evaluated from fitting is 38 ± 3 meV and 72 ± 3 meV for $CsPbBr_3$ and $CsPbCl_3$, respectively. The value is in good agreement with previous calculation results.[29] Since exciton absorption peak of $CsPbI_3$ could not be resolved at room temperature, a calculation value of ~ 20 meV from previous work was adopted in this work.[29] The binding energy decreases from 73 to *c.a.* 20 meV with the increase of halide elemental weight and the reduction of band gap from Cl to

I, which could be simply explained by perturbation theory.[51] The large exciton binding energy (E_b > 25 meV) confirm that in the as-grown all-inorganic lead halide perovskites exciton is stable and does not ionize into free carriers at room temperature, which well explains the observations of sharp exciton absorption peak and narrow band emission in absorption and emission spectroscopy (Fig. 1). The exciton binding energy of $CsPbX_3$ perovskite is relatively higher than II-VI and III-V semiconductors in the same spectra range (Supporting Information, Fig. S1). The underline reason is still unclear and further studies are needed.

The $CsPbX_3$ crystals with sub-wavelength thickness and uniform square shape naturally form high-quality whispering-gallery-mode microcavities. To probe the cavity performance for amplification and oscillations, we conducted lasing characterization with the nanoplatelets as schematically shown in Fig. 2a. At low pump fluence the band edge emission (FWHM: 20 nm, center wavelength: 527 nm) is too weak to be resolved in the same scale of the spectra taken above lasing threshold (Fig. 2a). When the pump fluence increases (~1.5 μJ/cm^2), narrow oscillation peaks can be observed around $\lambda = 530.0$ nm, which are the optical modes selectively amplified by the optical feedback in the square cavity. At a pump fluence of 2.5 μJ/cm^2 per pulse, the oscillation peak intensity increases sharply together with the further narrowing of peak width $\delta\lambda$, indicating the occurrence of lasing action. As the pumping fluence reaches 3.0 μJ/cm^2, the lasing linewidth (FWHM) is as small as $\delta\lambda = 0.15$ nm . The laser linewidth is relatively smaller compared to previous reports in semiconductor microscavities ($\lambda_l \sim 0.2$ nm). (Supporting Information, Tab. S1). The peak emission intensity versus excitation power (input-output curve) shows a typical "*S*" shape which confirms lasing action based on a multi-mode laser theory (Fig. 2d). The linear region at low pumping power is attributed to spontaneous emission, the superlinear increase region above 2.2 μJ/cm^2 suggests amplified spontaneous emission while the further linear increase region at higher

pump fluence demonstrates a full lasing action. The transition of linear region (spontaneous emission) towards nonlinear region (stimulated emission) occurs at P = 2.2 μJ/cm^2 which can be assigned as the lasing threshold. The carrier density at the threshold *c.a.*, ~ 1.5 ×10^{17}cm^{-3}, which is smaller the Mott density of $CsPbBr_3$ (~ 1.8 ×10^{17}cm^3), suggesting that the amplification of radiation is corresponding to excitonic lasing.[52] The slight blueshift of ~ 0.5 nm under intense pumping may be due to the reduction of refractive index.[52] The detailed mechanism needs further investigations.

Further investigations into the remarkable performance of the $CsPbBr_3$ platelet are conducted with time-resolved photoluminescence (TRPL) measurements (see Fig. 2e). The spontaneous emission lifetime is as long as τ_{SPE} ~4.2 ns at low excitation (~0.1P_{th}, navy dots). The τ_{SPE} decreases to ~3.0 ns at higher excitation fluence (~0.8P_{th}). When the excitation fluence is above the threshold (~1.2P_{th}), very fast time decay (< 30 ps, limited by the streak camera instrument response) dominates the kinetic process, further signifying the stimulated emission process and supporting the lasing occurrence in the square cavity.

We explore the optical modes inside the cavity. At the thickness of 180 nm, both of Fabry-Pérot (FP) mode oscillation between two facets and WGM oscillation among the four facets are possible. However, the gain threshold of FP mode is much larger than that of WGM oscillation. Therefore, primarily the lasing observed in experiment is considered to be due to WGM lasing. Further photoluminescence/lasing image and field calculations are conducted. Fig. 3a-3b shows the photoluminescence image of individual $CsPbBr_3$ below and above lasing threshold, respectively. When the excitation fluence is lower than the lasing threshold, the whole platelet body exhibits green color, suggesting the unidirectional out-coupling of spontaneous photoluminescence emission. While the excitation fluence is higher than the lasing threshold, the spontaneous emission is selected and confined by the whispering-gallery-mode cavity, large amount of photons can only emit from the square cavity edges, resulting in

a significantly stronger emission at the nanoplatelet edge and particularly at the corners. This pattern agrees very well with the electric field distributions of transverse mode (TM) calculated based on whispering-gallery-mode cavity using a finite domain time difference (FDTD) package (Fig. 3c). The calculation shows that the optical field at the resonance mode is well confined inside the microcavity in the form of WGM oscillation. The field has more leakage at four corners; therefore experimentally far-field emission image shows strong intensity in these areas.

We further investigate the lasing mode as a function of the nanoplatelet edge. With the increasing of nanoplatelet edge length L from 9.0 to 29.0 μm, the spacing between two adjacent mode decreases from to 3.0 nm to 0.9 nm (Fig. 3d). To rule out the influence of thickness difference on effective index around diffraction limit, $CsPbBr_3$ nanoplatelets with similar thickness (180±20 nm) were selected. The mode spacing extracted from Fig. 3d exhibit is linear proportional to the inverse of edge length (Fig. 3c-d). In a cubic WGM resonator, the mode spacing $\delta\lambda_l$ can be written as[53]:

$$\delta\lambda_l = \frac{\lambda_l^{\,2}}{2\sqrt{2}Ln_g} \ ,$$

A group refractive index n_g of ~ 3.7 is extracted out through the fitting, which show good agreement with previous studies, suggesting the achievement of whispering-gallery-mode lasing.[24] The lasing peaks usually locate at the lower energy side of spontaneous emission, which is widely observed in II-VI and III-V semiconductor microlasers. The phenomenon is assigned to exciton self-absorption during the photon propagation process along the cavity.[15] With the increasing of edge length, a small redshift of lasing peaks (~ 1.0 nm) was observed through compared the center frequency of the lasing modes, which also supports the occurrence of self-absorption.

Multi-color lasing actions can be realized in ternary and quaternary perovskite square-shaped platelet crystals at room temperature, as shown in Fig. 4a. When spontaneous emission colour of gain materials is tuned from blue to red through element modulation, the lasing threshold is around ~2.0-10.0 μJ/cm^2, which is comparable with traditional semiconductors and smaller than $CsPbX_3$ QDs WGM laser with much larger size as reported recently[15, 22]. The PL images (inset, Fig. 4a) above lasing threshold clearly show the predominance of whispering-gallery-modes lasing. The lasing peak is much stronger than their spontaneous emission background, indicating that large amount of spontaneous emission participates in lasing process. The high quality of square cavity and emission quantum yield are sustained for quaternary $CsPbX_3$ compounds. Fig. 4b displays zoom-in spectroscopy of one lasing mode for quaternary lead halide $CsPb(Br/I)_3$ perovskite with a centre emission wavelength of ~ 680 nm (Fig. 4b). In the solid state crystalline lasers, inhomogeneous broadening, such as Doppler and pressure broadening could be neglected.[54] The homogenous broadened lasing peak could be well fitted by a Lorentz function with FWHM of 0.14 nm.[25] The slight asymmetric profile is due to background subtraction. The laser linewidth is smallest among any single crystalline inorganic semiconductors and other perovskite microcavities in this spectra range (Supporting Information, Tab. S1). It should be noted that the laser linewidth of the as-grown perovskites is compared with or slightly lower than that of microlasers manufactured by embedding the semiconductor nanostructures into other ultra-low loss optical cavities such as silica whispering-gallery-mode cavities or distributed Bragg reflector cavities.[55, 56]It could be predicted that the laser linewidth of the all-inorganic perovskite micro-laser can be further promoted via introduction of the other high-*Q* passive optical cavities using similar methods. The high spectra coherence performance of as-fabricated microlaser can be attributed to room-temperature stable exciton as a result of large exciton binding energy, naturally formed cubic WGM mode resonator and promising highly luminescent gain materials.

To conclude, we demonstrate all-inorganic whispering-gallery-mode crystalline micro-cavities using van der Waals epitaxy cesium lead halide $CsPbX_3$ (X=Cl, Br, I), which show intense, high quality room-temperature spontaneous emission lasing tuned over the entire visible region (410-700 nm). Multi-colour, low-threshold lasing is realized in individual all-inorganic perovskite microcavities with promising spectra coherence. More efforts should be put on light-emission and electrically driven nanolaser sources development and also fundamental studies in macroscopic quantum optics such as exciton-photon polariton and polariton lasing.

Experimental Section

Synthesis of $CsPbX_3$ and characterization

The compounds $CsPbX_3$ perovskite nanoplatelets were grown by a vapour transport method using a home-built chemical vapour deposition (CVD) system. The substrate muscovite mica is cleaned by acetone and put inside the downstream of a quartz tube mounted in a single zone furnace (Lindberg/Blue MTF55035C-1). The source is mixed powder of lead halide PbX_2 and CsX with molar ratio 1:1. After the substrate and sources are placed inside the quartz tube, the quartz tube is pumped down with a setting base pressure of 50 mTorr, which is followed by a 30 sccm flow of high purity N_2 (99.999 %). The temperature and pressure inside the quartz tube are then set and stabilized for 20 minutes. For $CsPbCl_3$, $CsPbBr_3$, $CsPbI_3$, the temperature and pressure are 625 °C and 100 Torr, 575 °C and 50 Torr, 550 °C and 100 Torr, respectively. After the synthesis, the tube is cooled down naturally. The crystalline structure of as-grown nanoplatelets is characterized by x-ray diffraction (XRD, Bruker D8 advanced diffractometer, Cu Kα radiation). The size and thickness of the nanoplatelets are measured by scanning electron microscopy (SEM, JEOL JSM-7001F) and atomic force microscope (AFM, Veeco Dimension V).

Optical characterizations

The absorption spectroscopy of absorption spectroscopy was conducted on PerkimElmer Lambda 950 UV/ViS/NIR spectrometer. Steady-state photoluminescence was performed on a confocal micro-spectrometer using reflective symmetry (Horiba-JY T64000). For $CsPbBr_3$ to $CsPbI_3$ sample, A solid state diode laser 473 nm was focused by an objective (100×, NA: 0.9) to excite the samples. The pumping power is 22 μW. For $CsPbCl_3$ and $CsPb(Cl/Br)_3$, a UV 325 nm laser is focused by 20× UV objective as excitation source (power: 10 μW). The lasing and time-resolved PL spectroscopy was carried out on a home-built far-field epi-fluorescence

microscope at room temperature in a vacuumed atmosphere. A 400 nm pulsed laser was used as the excitation source, which was frequency doubled by a BBO crystal from an amplifier laser source (Libra, Coherent company, center wavelength: 800 nm, repetition rate: 1 kHz, pulse width: 50 fs). The pump light was focused by a microscopy objective (20×, NA: 0.45) and excited on the samples. The excitation laser spot was expanded (around 25 μm in diameter) to excite the whole nanoplatelets to minimize heat and optical damage at high energy pumping condition and promote energy injure efficiency. The emission signal was collected the same objective and analyzed by a Acton spectrometer (Spectra Pro 2500i) equipped with a Princeton Instrument liquid helium cooled CCD (Pixis 400B) for lasing measurement. For time-resolved photoluminescence measurement, the signal was analyzed by an Optronis Optoscope streak camera system with an ultimate temporal resolution up to ~ 10 ps.

Numerical calculations

The cross-section waveguide mode properties including effective indices and field distributions of nanoplatelet on top of mica were calculated using finite element method (Lumerical FDTD). To simplify the system from 3D to 2D, we introduce the effective index of refraction, mainly the planar waveguide model. Then, we simulate the mode distribution in 2D system using the effective index rather than the index of the material. The refractive index of mica and perovskite can be obtained from previous literature.[5]

Acknowledgements

Q. Z, R. S. and X. F. L. contributed the same to this work. Q.Z, R.S., X.F.L, T.C.S. and Q.X. conceived the idea and designed the experiment. Q. X. and Q. Z. gratefully acknowledge financial support from Singapore National Research Foundation (NRF) via Investigatorship award (NRF-NRFI2015-03) and a Competitive Research Program (NRF-CRP-6-2010-2), and Singapore Ministry of Education through two AcRF Tier 2 grants (MOE2011-T2-2-051 and MOE2015-T2-1-047). T.C.S. gratefully acknowledge the financial support from Nanyang Technological University start-up grant (M4080514), the Ministry of Education AcRF Tier 1 grant (RG101/15) and AcRF Tier 2 grants (MOE2013-T2-1-081 and MOE2014-T2-1-044); and the NRF through the Singapore-Berkeley Research Initiative for Sustainable Energy (SinBerRISE) CREATE Programme. Q.X. and T.C.S. also acknowledge the strong support from another Competitive Research Program grant (NRF2014NRF-CRP002-036).

Reference

[1] M. A. Green, A. Ho-Baillie, H. J. Snaith, *Nat. Photonics.* **2014**, *8*, 506-514.
[2] S. D. Stranks, H. J. Snaith, *Nat. Nanotechnol.* **2015**, *10*, 391-402.
[3] M. Gratzel, *Nat. Mater.* **2014**, *13*, 838-842.
[4] Q. Zhang, S. T. Ha, X. Liu, T. C. Sum, Q. Xiong, *Nano Lett.* **2014**, *14*, 5995-6001.
[5] G. Xing, N. Mathews, S. S. Lim, N. Yantara, X. Liu, D. Sabba, M. Gratzel, S. Mhaisalkar, T. C. Sum, *Nat. Mater.* **2014**, *13*, 476-480.
[6] Z.-K. Tan, R. S. Moghaddam, M. L. Lai, P. Docampo, R. Higler, F. Deschler, M. Price, A. Sadhanala, L. M. Pazos, D. Credgington, F. Hanusch, T. Bein, H. J. Snaith, R. H. Friend, *Nat. Nanotechnol.* **2014**, *9*, 687-692.
[7] L. Dou, Y. Yang, J. You, Z. Hong, W.-H. Chang, G. Li, Y. Yang, *Nat. Commun.* **2014**, *5*, 5405.
[8] F. Deschler, M. Price, S. Pathak, L. E. Klintberg, D.-D. Jarausch, R. Higler, S. Hüttner, T. Leijtens, S. D. Stranks, H. J. Snaith, M. Atatüre, R. T. Phillips, R. H. Friend, *J Phys. Chem. Lett.* **2014**, *5*, 1421-1426.
[9] Q. A. Akkerman, V. D'Innocenzo, S. Accornero, A. Scarpellini, A. Petrozza, M. Prato, L. Manna, *J. Am. Chem. Soc.* **2015**, *137*, 10276-10281.
[10] S. T. Ha, X. Liu, Q. Zhang, D. Giovanni, T. C. Sum, Q. Xiong, *Adv. Opt. Mater.* **2014**, *2*, 838-844.
[11] H. Zhu, Y. Fu, F. Meng, X. Wu, Z. Gong, Q. Ding, M. V. Gustafsson, M. T. Trinh, S. Jin, X. Y. Zhu, *Nat. Mater.* **2015**, *14*, 636-642.
[12] A. Brehier, R. Parashkov, J. S. Lauret, E. Deleporte, *Appl. Phys. Lett.* **2006**, *89*, 171110.
[13] G. Lanty, A. Bréhier, R. Parashkov, J. S. Lauret, E. Deleporte, *New. J. Phys.* **2008**, *10*, 065007.
[14] K. J. Vahala, *Nature* **2003**, *424*, 839-846.
[15] X. Liu, Q. Zhang, Q. Xiong, T. C. Sum, *Nano Lett.* **2013**, *13*, 1080-1085.
[16] Y. S. Zhao, A. Peng, H. Fu, Y. Ma, J. Yao, *Adv. Mater.* **2008**, *20*, 1661-1665.
[17] A. Pan, W. Zhou, E. S. P. Leong, R. Liu, A. H. Chin, B. Zou, C. Z. Ning, *Nano Lett.* **2009**, *9*, 784-788.
[18] L. Mahler, A. Tredicucci, F. Beltram, C. Walther, J. Faist, B. Witzigmann, H. E. Beere, D. A. Ritchie, *Nat. Photonics.* **2009**, *3*, 46-49.
[19] D. W. Snoke, A. J. Shields, M. Cardona, *Phys. Rev. B* **1992**, *45*, 11693-11697.
[20] A. L. Schawlow, C. H. Townes, *Phys. Rev.* **1958**, *112*, 1940-1949.
[21] R. Agarwal, C. J. Barrelet, C. M. Lieber, *Nano Lett.* **2005**, *5*, 917-920.
[22] S. Yakunin, L. Protesescu, F. Krieg, M. I. Bodnarchuk, G. Nedelcu, M. Humer, G. De Luca, M. Fiebig, W. Heiss, M. V. Kovalenko, *Nat. Commun.* **2015**, *6*, 8056.
[23] R. Chen, B. Ling, X. W. Sun, H. D. Sun, *Adv. Mater.* **2011**, *23*, 2199-2204.
[24] H. Baek, C.-H. Lee, K. Chung, G.-C. Yi, *Nano Lett.* **2013**, *13*, 2782-2785.
[25] S. Wu, S. Buckley, J. R. Schaibley, L. Feng, J. Yan, D. G. Mandrus, F. Hatami, W. Yao, J. Vuckovic, A. Majumdar, X. Xu, *Nature* **2015**, *520*, 69-72.
[26] D. G. Lidzey, D. D. C. Bradley, A. Armitage, S. Walker, M. S. Skolnick, *Science* **2000**, *288*, 1620-1623.
[27] D. G. Lidzey, D. D. C. Bradley, M. S. Skolnick, T. Virgili, S. Walker, D. M. Whittaker, *Nature* **1998**, *395*, 53-55.
[28] M. Kulbak, D. Cahen, G. Hodes, *J. Phys. Chem. Lett.* **2015**, *6*, 2452-2456.
[29] L. Protesescu, S. Yakunin, M. I. Bodnarchuk, F. Krieg, R. Caputo, C. H. Hendon, R. X. Yang, A. Walsh, M. V. Kovalenko, *Nano Lett.* **2015**, *15*, 3692-3696.
[30] Y. Wang, X. Li, J. Song, L. Xiao, H. Zeng, H. Sun, *Adv. Mater.* **2015**, *27*, 7101-7108.
[31] D. Zhang, S. W. Eaton, Y. Yu, L. Dou, P. Yang, *J. Am. Chem. Soc.* **2015**, *137*, 9230-9233.
[32] Y. Bekenstein, B. A. Koscher, S. W. Eaton, P. Yang, A. P. Alivisatos, *J. Am. Chem. Soc.* **2015**, *137*, 16008-16011.

[33] Q. A. Akkerman, S. G. Motti, A. R. Srimath Kandada, E. Mosconi, V. D'Innocenzo, G. Bertoni, S. Marras, B. A. Kamino, L. Miranda, F. De Angelis, A. Petrozza, M. Prato, L. Manna, *J. Am. Chem. Soc.* **2016**, *138*, 1010-1016.

[34] Y. Zhu, Y. Zhou, M. I. Utama, M. de la Mata, Y. Zhao, Q. Zhang, B. Peng, C. Magen, J. Arbiol, Q. Xiong, *Nanoscale* **2013**, *5*, 7242-7249.

[35] M. I. B. Utama, M. de la Mata, C. Magen, J. Arbiol, Q. Xiong, *Adv. Funct. Mater.* **2013**, *23*, 1636-1646.

[36] M. I. Utama, Z. Peng, R. Chen, B. Peng, X. Xu, Y. Dong, L. M. Wong, S. Wang, H. Sun, Q. Xiong, *Nano Lett.* **2011**, *11*, 3051-3057.

[37] C. K. Moller, *Nature* **1958**, *182*, 1436.

[38] P. Gehring, B. F. Gao, M. Burghard, K. Kern, *Nano Lett.* **2012**, *12*, 5137-5142.

[39] H. Li, J. Cao, W. Zheng, Y. Chen, D. Wu, W. Dang, K. Wang, H. Peng, Z. Liu, *J. Am. Chem. Soc.* **2012**, *134*, 6132-6135.

[40] Y. Shi, W. Zhou, A. Y. Lu, W. Fang, Y. H. Lee, A. L. Hsu, S. M. Kim, K. K. Kim, H. Y. Yang, L. J. Li, J. C. Idrobo, J. Kong, *Nano Lett.* **2012**, *12*, 2784-2791.

[41] M. I. Utama, F. J. Belarre, C. Magen, B. Peng, J. Arbiol, Q. Xiong, *Nano Lett.* **2012**, *12*, 2146-2152.

[42] Y. Zhou, Y. Nie, Y. Liu, K. Yan, J. Hong, C. Jin, Y. Zhou, J. Yin, Z. Liu, H. Peng, *ACS Nano* **2014**, *8*, 1485-1490.

[43] S. Hirotsu, J. Harada, M. Iizumi, K. Gesi, *J. Phys. Soc. Jpn.* **1974**, *37*, 1393-1398.

[44] D. M. Trots, S. V. Myagkota, *J. Phys. Chem. Solids* **2008**, *69*, 2520-2526.

[45] C. H. P. Y. H. Chang, *J. Korean. Phys. Soc.* **2004**, *44*, 889-893.

[46] M. Grundmann, in *An Introduction Including Nanophysics and Applications*, Springer-Verlag Berlin Heidelberg, Berlin **2010**.

[47] G. Moody, C. Kavir Dass, K. Hao, C.-H. Chen, L.-J. Li, A. Singh, K. Tran, G. Clark, X. Xu, G. Berghauser, E. Malic, A. Knorr, X. Li, *Nat. Commun.* **2015**, *6*.

[48] V. D'Innocenzo, G. Grancini, M. J. Alcocer, A. R. Kandada, S. D. Stranks, M. M. Lee, G. Lanzani, H. J. Snaith, A. Petrozza, *Nat. Commun.* **2014**, *5*, 3586.

[49] T. Byrnes, N. Y. Kim, Y. Yamamoto, *Nat. Phys.* **2014**, *10*, 803-813.

[50] GrossoG, GravesJ, A. T. Hammack, A. A. High, L. V. Butov, HansonM, A. C. Gossard, *Nat. Photonics.* **2009**, *3*, 577-580.

[51] J. H. Choi, P. Cui, H. Lan, Z. Zhang, *Phys. Rev. Lett.* **2015**, *115*, 066403.

[52] N. F. Mott, *Rev. Mod. Phys.* **1968**, *40*, 677-683.

[53] A. K. Bhowmik, *Appl. Opt.* **2000**, *39*, 3071-3075.

[54] O. Svelto, in *Principles of Lasers*, Springer, **2010**, pp. 505-545.

[55] Y. Chu, A. M. Mintairov, Y. He, J. L. Merz, N. A. Kalyuzhnyy, V. M. Lantratov, S. A. Mintairov, *Phys. Lett. A* **2009**, *373*, 1185-1188.

[56] A. Woolf, T. Puchtler, I. Aharonovich, T. Zhu, N. Niu, D. Wang, R. Oliver, E. L. Hu, *Proc. Natl. Acad. Sci.* **2014**, *111*, 14042-14046.

Figures

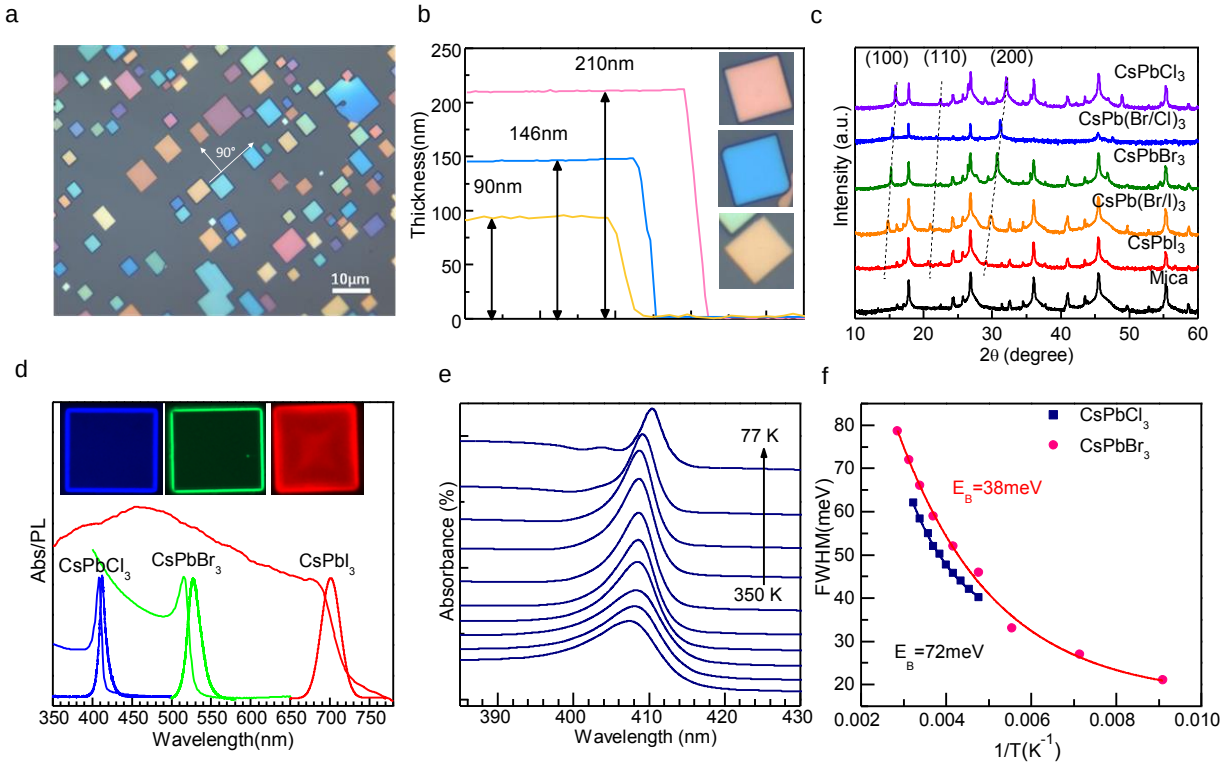

Figure 1 Cesium Lead Halide Perovskite Nanoplatelets. (**a**) Optical image of $CsPbBr_3$ nanoplatelets showing square or rectangular shapes and rich colors. (**b**) AFM characterization of individual $CsPbBr_3$ nanoplatelets with different colors. (**c**) XRD pattern of as-grown $CsPbX_3$ nanoplatelets showing cubic phase. (**d**) Optical absorption (dash line) and PL spectra (solid line) of $CsPbCl_3$, $CsPbBr_3$ and $CsPbI_3$ nanoplatelets. Inset: PL image of $CsPbCl_3$, $CsPbBr_3$ and $CsPbI_3$ (left to right). (**e**) Temperature dependent absorption spectra of $CsPbCl_3$. The temperature for the curve from bottom to up is from 350 K, 330 K, 320 K, 296 K, 260 K, 230 K, 210 K, 200 K, 160 K, 120 K and 77 K, respectively. (**f**) The full width at half maximum (FWHM) of the curve or the bandwidth of the exciton peak dependent on temperature for $CsPbBr_3$ (pink) and $CsPbCl_3$ (navy). A single exponential decrease function (lines) is used to fit the experimental data (dots). The exciton binding energy evaluated from the fitting for $CsPbBr_3$ and $CsPbCl_3$ is 38 meV and 72 meV, respectively.

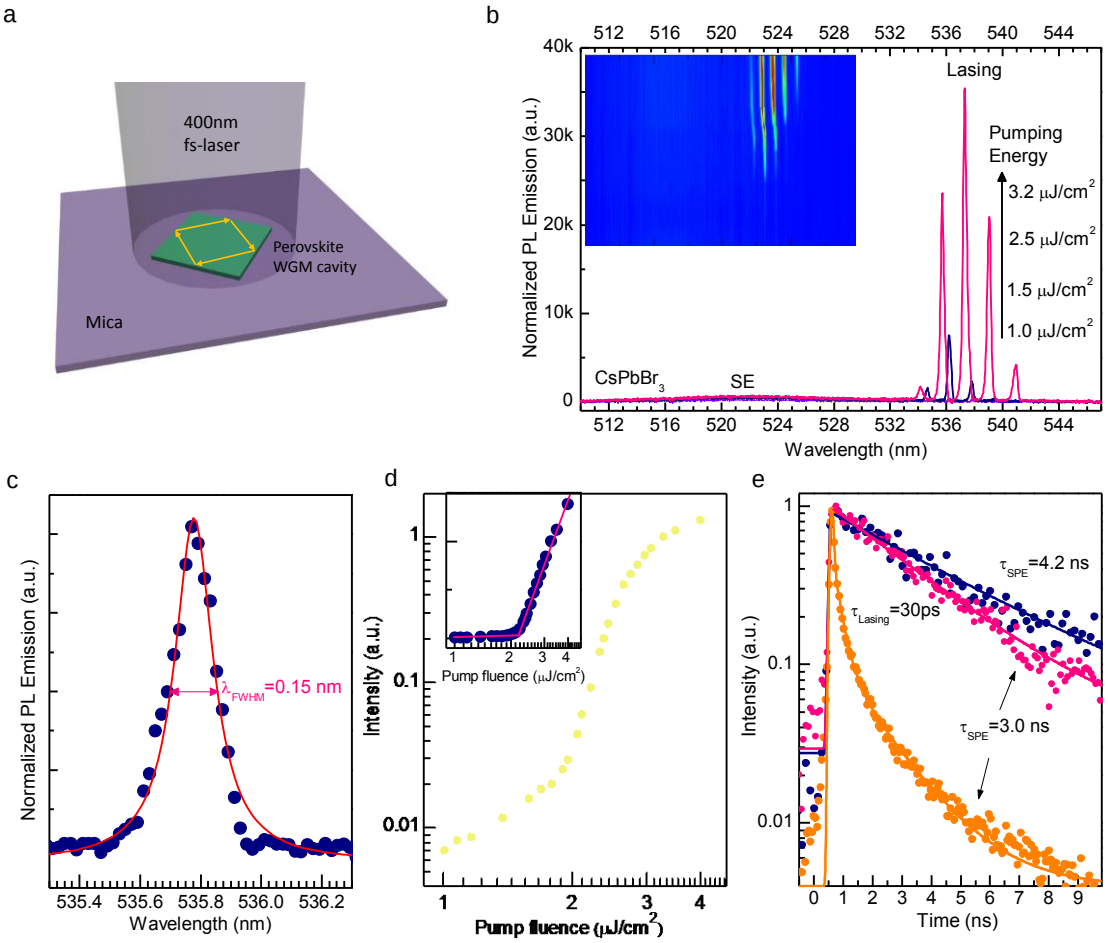

Figure 2 Lasing Characterization of Cesium Lead Halide Nanoplatelets. (a) Schematic of a $CsPbX_3$(X= Cl, Br or I) plate on mica substrate pumped by a 400 nm laser excitation (~50 fs, 1 kHz). The yellow line indicates the light propagation inside the cubic WGM cavity. (b) Emission spectra at five different optical pump fluencies, showing the transition from spontaneous emission to amplified spontaneous emission and to lasing. Inset: 2D pseudo-color plot of the plate emission spectra under different pump fluence (P) showing a broad SPE peak below the threshold (P_{th}) of ~2.2 μJ/cm^2.pulse and a series narrow lasing peaks above the threshold. (c) A Lorentz fitting of a lasing oscillation mode. The FWHM is 0.15 nm. (d) Nonlinear response of laser output power with increasing pump fluence, showing threshold region as a 'kink' between the two linear regions of spontaneous emission and lasing (Inset). The lasing energy at the 'kink' (P_{th}) is of ~ 2.2 μJ/cm^2.pulse. (e) TRPL decay kinetics after photoexcitation with pump fluence below (P ~0.8P_{th}) and above threshold (~1.2 P_{th}), showing a ~3.0 ns SPE decay process below P_{th} and a <30 ps lasing process above P_{th}. A lifetime of ~4.2 ns is shown at relatively low pump fluence (~0.1 P_{th}).

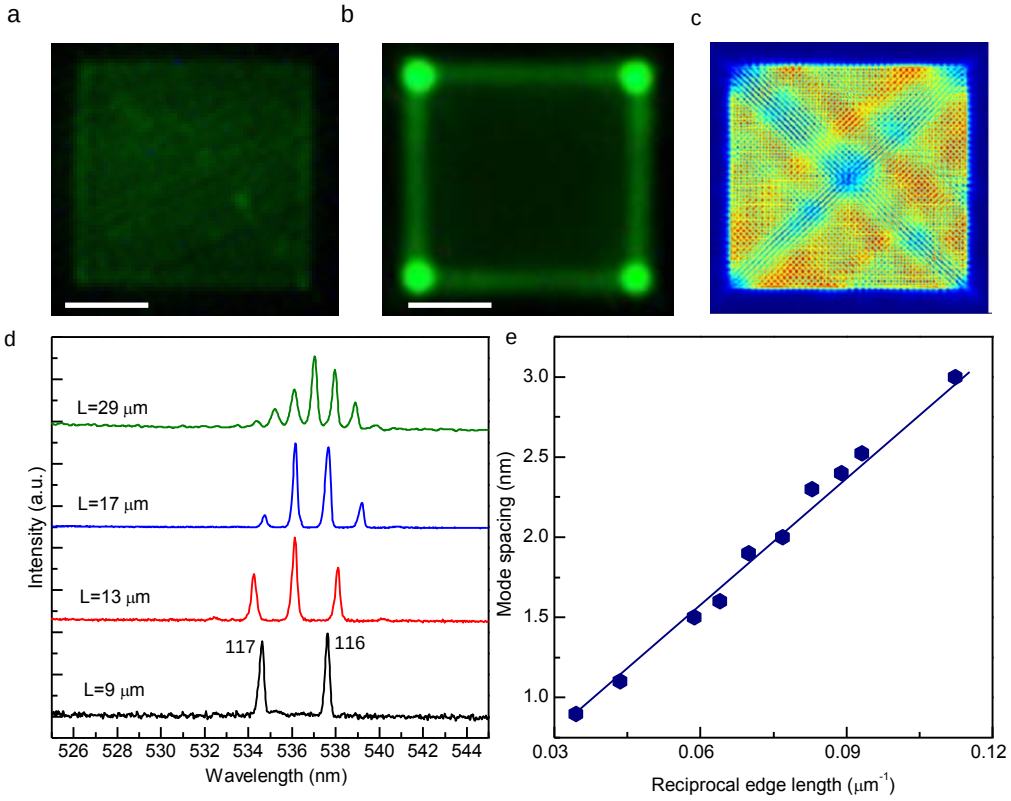

Figure 3 Whispering-Gallery-Mode Characterization and Numerical Calculation. (a-b) Photoluminescence emission image captured by a charge coupled detector using a reflective symmetry below (a) and above (b) lasing threshold for an individual $CsPbBr_3$ perovskite nanoplatelet. The thickness and the edge length of the nanoplatelet is around 180 nm and 9 μm, respectively. The scale bar is 3 μm. The excitation laser is a femto-second laser with wavelength of 400 nm and spot size is large enough to illuminate the whole nanoplatelet. The green color shows photoluminescence coupled out from the nanoplatelet. Below the lasing threshold, the whole body of nanoplatelet is in green, indicating unidirectional spontaneous emission. Above the lasing threshold, the edge emission is much stronger than the center area and the four corners have strongest emission, suggesting the confinement effect and mode selection by the whispering-gallery-mode cavity. (c) Simulated electric field distribution inside the square perovskite cavity under a transverse magnetic resonant mode. The pattern shows that whispering-gallery-mode is supported by the cavity. Four corners show the strongest out-coupling or leakage compared with the other places. (d) Multi-mode lasing spectroscopy of four nanoplatelets with different edge length from 9 to 29 μm. The oscillation number of lasing mode (9 μm) is indicated along with the spectroscopy. The edge length is indicated nearby each spectroscopy. The selected four nanoplatelets have similar thickness nanoplatelets are almost the same (±20 nm). The spacing between two adjacent modes decreases with the increasing of edge length. (e)

The mode spacing is extracted out and plotted as a function of the inverse of edge length. Navy dots are experimental data. Navy line is the linear function fitting of the experimental data.

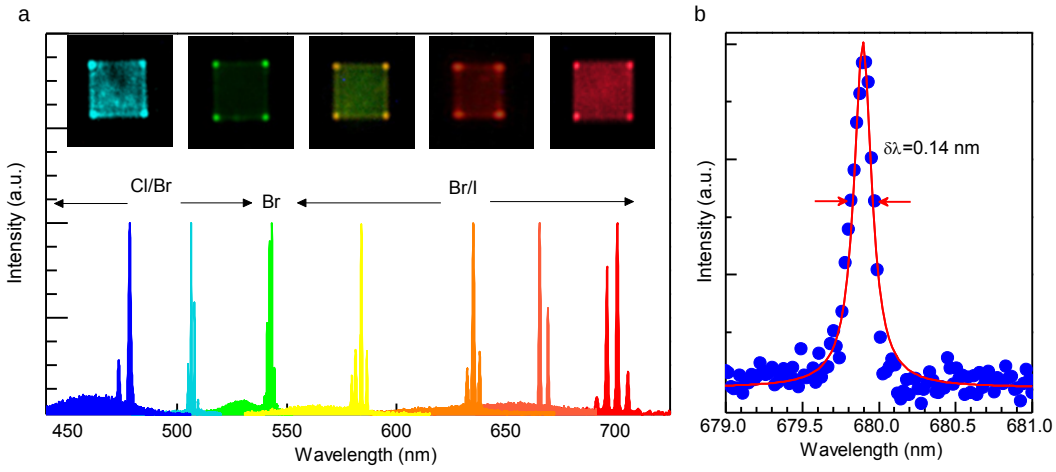

Figure 4 Multi-color whispering-gallery-mode microlaser based on inorganic perovskites with high-quality factor. (a) Lasing spectroscopy and image of individual $CsPbX_3$ perovskite nanoplatelet with different halide ion. Left to right shows the halide X varies from Cl_aBr_{3-a}, Br to Br_aI_{3-a}. The emission images above lasing threshold are inset from Cl_aBr_{3-a}, Br to Br_aI_{3-a}, in according with lasing spectroscopy. (b) Zoomed in spectroscopy of a lasing mode of $CsPbBr_aI_{3-a}$. The dots and line are experimental data and Lorentz function fitting curve, respectively. The full width at half maximum of the laser mode is 0.14 nm.